Ultrastructure of Poly(*p*-phenylenebenzobisoxazole) Fibers

David C. Martin[†] and Edwin L. Thomas*[,‡]

Polymer Science and Engineering, The University of Massachusetts at Amherst, Amherst, Massachusetts 01003

Received April 11, 1990; Revised Manuscript Received October 29, 1990

ABSTRACT: The ultrastructure of poly(*p*-phenylenebenzobisoxazole) (PBZO or PBO) was studied as a function of processing condition by wide-angle X-ray scattering (WAXS), selected-area electron diffraction (SAED), dark-field transmission electron microscopy (DF), and high-resolution electron microscopy (HREM). The development of single-crystal texturing in thin films made it possible to index the PBZO scattering patterns to a nonprimitive ($N = 2$) monoclinic space group Pc (No. 7). The new unit cell parameters are $a = 1.120$ nm, $b = 0.354$ nm, $c = 1.205$ nm, $\gamma = 101.3°$, and $\rho_{xl} = 1.66$ g/cm^3, with neighboring chains in the a direction placed at relative axial translations of $\pm^1/_4c$. HREM images of the 0.55-nm (200) and 0.35-nm (010) lateral spacings between PBZO molecules enabled the crystallite size, shape, and relative orientations to be directly determined. Defects within and between PBZO crystallites were observed, and molecular models are presented that are consistent with these observations.

A. Introduction

The rigid-rod polymers poly(*p*-phenylenebenzobisthiazole) (PBZT) and poly(*p*-phenylenebenzobisoxazole) (PBZO or PBO) are of considerable interest for high-performance applications. The chemical structures of PBZT and PBZO are shown in Figure 1. Historically, more effort has been expended in refining the spinning and processing steps for PBZT fiber because it was originally easier to obtain higher molecular weight PBZT than PBZO. However, recent advances in synthetic techniques have made it possible to reproducibly obtain high molecular weight PBZO[1] and PBZO is now under commercial development by Dow Chemical Co. It is therefore reasonable to expect an expanded interest in the relationship between structure and properties of PBZO fiber.

We investigated the ultrastructure of *cis*-PBZO fiber by wide-angle X-ray scattering (WAXS), selected-area electron diffraction (SAED), dark-field transmission electron microscopy (DF), and high-resolution electron microscopy (HREM). The morphology was examined as a function of postspinning heat treatment of the PBZO fiber.

Our interest concerns the molecular ordering that occurs in as-spun PBZO fiber and its evolution during tensioned heat treatment. Information about the size, shape, orientation, and internal perfection of PBZO crystallites is important for a full understanding of the unique mechanical properties of these materials. In particular, the tensile moduli of the best PBZO fibers (320 GPa) are now approaching values expected theoretically (730 GPa) from semiempirical AM1 molecular orbital calculations of isolated molecules.[2] The extremely high tensile moduli and strengths of rigid-rod polymer fibers suggests that understanding and possibly controlling morphological defects (such as the dislocations within and grain boundaries between crystalline domains) may be critical for further optimizing properties.

B. Background

The structure of PBZO fiber was first studied by WAXS by Won Choe and Kim.[3] The WAXS pattern of the as-spun fiber showed good orientation, with two strong equatorial reflections at spacings of 0.555 and 0.335 nm and weak scattering on the first and third layer lines (1.135 nm) along the fiber direction.

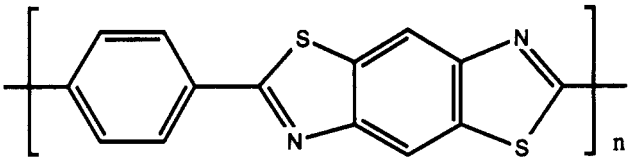

PBZT

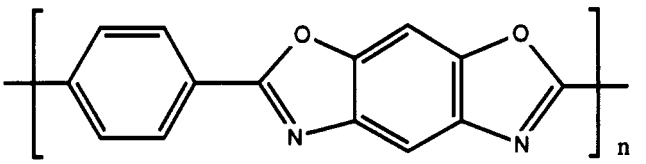

PBZO

Figure 1. Chemical structures of *trans*-PBZT and *cis*-PBZO.

Model calculations by Bhaumik et al.[4] using an empirical molecular orbital approach for the interactions between *cis*-PBZO molecules showed that there is a minimum in the energetic interactions between neighboring PBZO monomers at a characteristic axial shift of 0.2 nm for molecules packed side by side (0.62 nm apart) and at 0.3 nm for molecules packed face to face (0.35 nm apart).[4] However, the energy troughs as a function of relative axial position were shallow (3 kcal/mol; 5 kT), so it might be expected that PBZO molecules would exhibit axial disorder in the solid state as does PBZT.[5]

The study of Bhaumik et al.[4] did not investigate the effect of different internal conformations of the *cis*-PBZO molecule. The energetics of the interactions between neighboring PBZO molecules might be quite sensitive to internal rotations of the heterocyclic group about the chain axis. For *cis*-PBZO, the interactions between neighboring molecules may be particularly sensitive to such internal rotations because of the chemical dipole induced within the heterocyclic ring by the different electronegativities of nitrogen and oxygen. For "trans" arrangements these dipoles are in opposite directions and tend to locally cancel. In the "cis" arrangement the dipoles are both in the same direction and locally add. This makes the local net dipole of a cis monomer stronger, so therefore the intermolecular interactions should be of longer range.

[†] Current address: Materials Science and Engineering, The University of Michigan, H. H. Dow Building, Ann Arbor, MI 48109.
[‡] Current address: Program in Polymer Science and Technology, Massachusetts Institute of Technology, Room 13-5066, Cambridge, MA 02139.

0024-9297/91/2224-2450$02.50/0

The crystal structure of PBZO was first deduced from WAXS scattering by Fratini and Adams.[6] A primitive, monoclinic unit cell was found with parameters $a = 0.565$ nm, $b = 0.358$ nm, $c = 1.174$ nm, $\alpha = 90°$, and $\gamma = 102.5°$. This unit cell gives a density of 1.64 gm/cm^3, which is not much different from that observed experimentally (1.56 gm/cm^3). Also, it explains the expected close packings of PBZO molecules "side to side" at 0.55 nm in the a direction and "face to face" at 0.35 nm in the b direction.

The microstructure of PBZO was studied in detail by Adams et al.[7] and by Krause et al.[8] WAXS and SAED scattering patterns of PBZO fiber indicated strong equatorial reflections and layer line scattering consistent with the high degree of orientation and good lateral packing of the PBZO molecules. The development of three-dimensional crystallinity was evidenced by the development of localized scattering on upper order layer lines. Adams et al.[7] suggested that the primitive unit cell of Fratini and Adams[6] was consistent with WAXS diffractometer data, but a detailed comparison of the predicted scattering intensity from this unit cell with that obtained experimentally was not presented. In particular, the strong reflections on the second-order layer line corresponding to the development of three-dimensional crystallinity were not indexed in terms of this unit cell assignment.

Another feature in the scattering behavior of PBZO that is apparent from the data of Adams et al.[7] and Krause et al.[8] but that has not received attention is the notable lack of scattered intensity at the meridian on the second-order layer line. Such a lack of scattered intensity may be explained by either a systematic absence due to symmetry in the lattice factor or the presence of a weak molecular transform at this scattering angle.

SAED studies showed that the relative intensity of the first and second equatorial reflections was sensitive to the region of sample investigated.[8] This is indicative of a domain structure formed from texturing within the PBZO fiber. Azimuthal scans of the equatorial reflections[7] indicated a misorientation of 6° in the as-spun case and 4° in the heat-treated case in both WAXS and SAED, confirming that misorientation was present down to very local size scales (1 μm or less) in the fiber.

Scatter plots of the crystal sizes observed in equatorial DF showed a rather broad distribution in both axial and lateral size.[7] The mean crystal dimensions were seen to increase in both the lateral and axial directions, but the ratio of the average axial size to average lateral size of the crystallites decreased from 0.90 to 0.55 after heat treatment. Apparently, the growth of the PBZO crystallites in the axial direction is not as extensive as growth in the lateral direction. This is in contrast to heat-treated PBZT,[8] where crystallites have an average axial size to average lateral size ratio of 1.7.

SAXS patterns of heat-treated PBZO fiber exhibit a weak four-point pattern.[7,9] These results indicate the development of periodic fluctuations in electron density at specific angles to the fiber axis. Similar four-point patterns have been seen in SAXS of fibers of ABPBO, a semiflexible polymer that shows well-developed three-dimensional crystallinity. This behavior is in sharp contrast to that of heat-treated PBZT, which does not exhibit four-point SAXS behavior.[10] Adams et al.[7] propose a model of tilted lamellar crystallites to explain this four-point SAXS behavior, but it is known from DF that such lamellar crystallites do not exist in PBZO. A more detailed explanation of the four-point SAXS scattering in terms of specific morphological features present in PBZO and absent in PBZT has not yet been advanced.

Table I
Characteristics of PBZO Fiber[14]

designation (Dow code)	HT, °C	color	modulus, GPa	strength, GPa	elong, %
AS-383-C8601037-69E	AS	yellow	165	4.3	2.8
HT-383-C8700357-8A	600	orange	317	4.9	1.7
HT-383-C8700357-8B	665	purple	289	3.0	1.2

The first HREM study of PBZO fiber was recently published by Adams et al.[11] The critical dose J_c was reported to be 0.2 C/cm^2 for 200-kV electrons. The ~0.55-nm fringes were clearly visible in the HREM image, with orientation of the molecules in the direction of the fiber maintained over large regions (at least 500 nm) of the micrograph. Evidence for ~0.35-nm fringes was seen in the optical transform, but these fringes were difficult to resolve on the micrograph. The sizes, shapes, and relative positions of different PBZO crystallites could be detected (of size approximately 5 nm × 10 nm), but the limited field of view made statistically significant values difficult to establish. A defective region was shown where the 0.55-nm fringes lined up properly on one side of the image but did not line up properly on the other side. Although these data suggest the presence of a dislocation within the PBZO crystallite, a specific model that explained the structure of the defect was not presented.

Young et al. have investigated the morphology of PBZO and obtained evidence for orientation texturing within thin sections microtomed parallel to the fiber axis.[12] They also reported qualitative evidence for a skin–core effect, with the orientation of the molecules near the fiber core less perfect than those near the skin. During heat treatment, an increase in the crystallinity of the core regions was observed. Again, discrete (hkl) reflections were seen in WAXS and SAED and interpreted in terms of an increase in three-dimensional crystallinity, but a model for the packing of the PBZO molecules within the unit cell was not presented.

In the most recent WAXS investigation of PBZO crystal structure by Fratini et al., a nonprimitive unit cell with $a = 11.20$ (1), $b = 3.540$ (2), and $c = 12.050$ (3) nm and $\gamma = 101.3$ (1)° was determined.[13] The possibility of regular axial translations between neighboring molecules in the a direction was investigated by using the linked-atom least squares (LALS) approach. It was determined that translations of $^1/_{10}c$ and $^1/_2c$ were energetically feasible, with the $^1/_{10}c$ placement giving the lowest R factor of 0.114. A placement of $^3/_{10}c$ was also considered but gave a higher R factor. During the refinement, 11 different experimentally obtained structure factor amplitudes were compared with model predictions.

C. Experimental Section

The *cis*-PBZO fiber used in this study was spun by Dow Chemical Co. and provided to us by W. W. Adams of WPAFB. The samples received were as-spun (AS), heat-treated at 600 °C (HT 600), and heat-treated at 665 °C (HT 665). The mechanical properties of the material as reported by Dow Chemical[14] are listed in Table I.

Fiber samples were wound on small (10 mm) cardboard supports and Cu Kα WAXS patterns were obtained of the corresponding bundles. The X-ray negatives were scanned with an Optronics P-1000 digitizing microdensitometer. The maximum optical density of the scanned negatives was less than one so that the relationship between scattered beam intensity and film darkening remained linear.

Samples for TEM study were prepared by the "detachment replication" procedure.[10,15] HREM images of the detached fragments supported on holey carbon films were obtained by using low-dose procedures. The utility of HREM techniques for

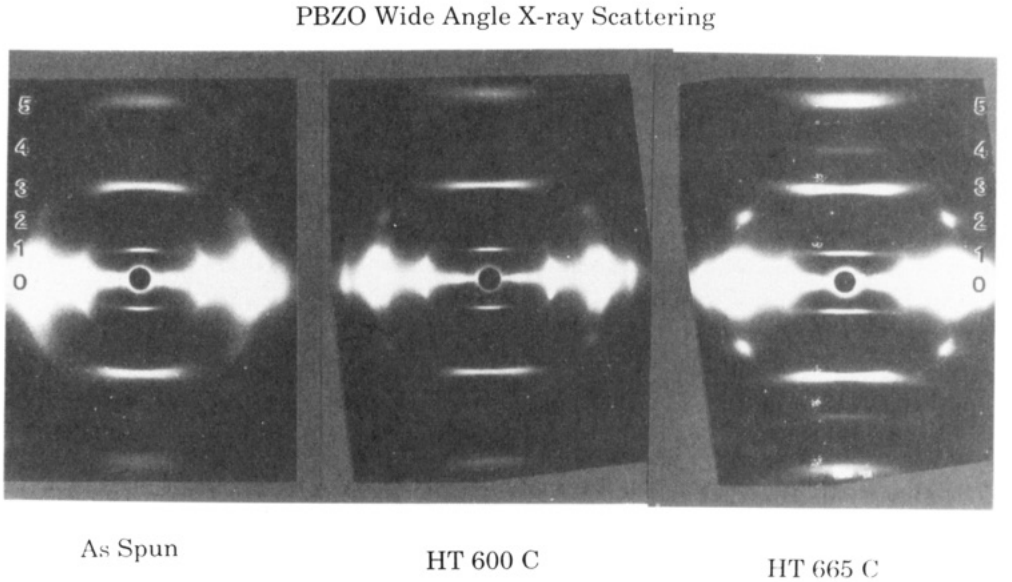

Figure 2. WAXS of PBZO fiber bundles as a function of heat treatment. The patterns exhibit strong equatorial reflections indicative of good lateral packing and layer lines indicative of high molecular orientation but with a certain degree of disorder between molecules. A striking feature is a sharp off-meridion reflection on the second layer line, which becomes more prominent after heat tratment. This reflection indicates the development of three-dimensional crystalline ordering.

studying polymer microstructures is reviewed elsewhere.[15,16] Typically, a magnification of 100000× and exposure time of less than 1 s was used. These conditions correspond to a total sample dose of less than 0.1 C/cm^2. Examination of the SAED pattern with a lower beam flux after exposure revealed that the equatorial reflections could still be resolved. The HREM images were recorded on Kodak SO-163 electron image film, developed in full strength D-19 developer for 12 min.

The presence and spacing of fringes in low-dose HREM images were determined with a He/Ne laser optical bench, calibrated with lattice images of the 0.34-nm spacing in graphite taken at the same magnification. The optical diffractograms were obtained on Kodak Type 55 film, which produces both a positive and a negative. The negatives were scanned and examined to determine the angular broadening of reflections in the optical transform.

D. Results

1. WAXS and SAED Scattering. Figure 2 shows WAXS patterns of fiber bundles of PBZO as a function of heat treatment. In these patterns the fiber axes are oriented vertically. The presence of "layer lines" perpendicular to the axis of orientation indicates that there is a substantial amount of axial disorder in PBZO, similar to PBZT. However, a striking feature of the WAXS patterns is the strong off-meridian reflection on the second-order layer line, which becomes more intense and localized with increasing heat treatment. This reflection is indicative of 3-D crystallinity in the heat-treated PBZO material. This reflection was also observed in the studies by Adams et al.[7] and Krause et al.[8]

It can also be noted from Figure 2 that the PBZO WAXS patterns do NOT exhibit strong scattering on the meridian on the second-order layer line. Furthermore, the scattering on the first layer line is much broader in the lateral direction ($\delta k \sim 3$ nm^{-1}) than the strong reflection on the second-order layer line ($\delta k \sim 0.3$ nm^{-1}).

Figure 3 shows plots of the WAXS data obtained by scanning the negatives with a Optronics P-1000 microdensitometer. Figure 3a shows scans along the meridian plotted as a function of scattering vector k. Figure 3b shows scans along the second layer line, plotted as a function of R, the cylindrical coordinate of the reciprocal lattice corresponding to the projection of the scattering vector k on the equatorial plane. These data were obtained by averaging the intensity within a rectangular window of width 0.8 nm^{-1} oriented along the meridian and the second-order layer line. Note in Figure 3a the strong peaks corresponding to the (001) and (003) layer lines. During heat treatment the peaks narrow and move in slightly. This is indicative of an increase in the crystalline ordering along the chain and a small increase in the c dimension. Also note that the scattering at (002) is absent to within the background level. In Figure 3b the increase in intensity and localization of the strong peak at a position R of 2.6 nm^{-1} with heat treatment is evident.

Figure 4 shows schematic drawings of SAED patterns of thin sections of PBZO. As in the study by Krause et al.,[8] it was found that during SAED observation of PBZO fiber fragments the relative intensity of the first and second equatorial reflections was not constant, indicating that orientation texturing was present. While studying different regions of PBZO fiber fragments by SAED, we noted that the strong off-axis reflections on the second-order layer line and the first and fourth equatorial reflections, corresponding to first and second orders of the 0.55-nm spacing, were always visible at the same time. Furthermore, it was possible to locate extremely thin sections of PBZO fiber fragments in which the texturing was so strong that the first and fourth equatorial reflections were present but the second and third reflections were completely missing. Figure 4 shows schematics of SAED patterns from thick and thin sections of PBZO. In thick sections all of the equatorial reflections are visible and the SAED patterns correspond to the WAXS data presented in Figure 2. However, in the thinnest sections only the (h00) set of reflections were seen on the equator. Since the (00l) direction is in the fiber direction, this indicates "single-crystal" texturing in the thin regions about the [010] zone axis. Nevertheless, in these thin sections there remained localized scattering on the second layer line.

These observations indicate that the off-axis reflections on the second-order layer line are in the crystal zone containing the 0.55-nm packing direction; i.e., these reflections represent regular ordering between PBZO molecules in the a direction.

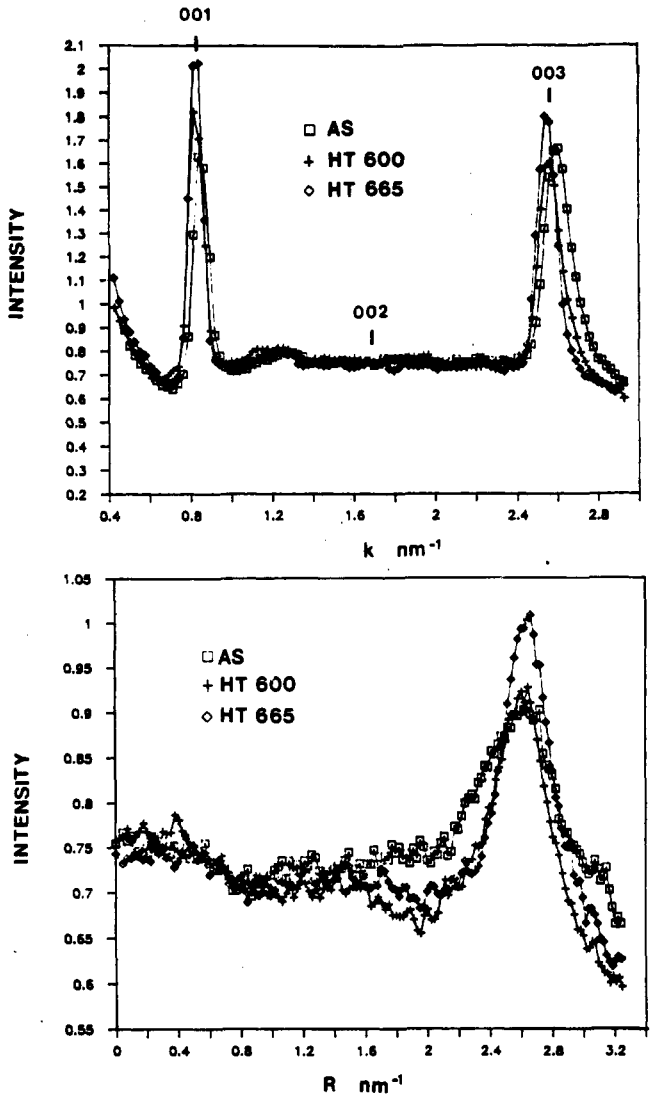

Figure 3. Densitometer scans of the WAXS data presented in Figure 2. (a, Top) Meridional scan showing the average WAXS intensity in a rectangular window of width 0.8 nm^{-1} oriented along the fiber axis, plotted as a function of magnitude of the scattering vector k. (b, Bottom) Scan of the second-order layer line, again using a rectangular window of width 0.8 nm^{-1} centered about the layer line, plotted as a function of the cylindrical reciprocal lattice coordinate R.

Further inspection of the PBZO SAED scattering pattern shows that the localized reflections on the second layer line correspond to intermediate positions of the strong 0.55-nm equatorial reflections. Specifically, the reflections on $l = 2$ occur at positions corresponding to (102) and (302) when the first and fourth equatorial reflections are indexed as (200) and (400). This indexing scheme requires a nonprimitive PBZO unit cell with two chains per lattice site. Although the (102) reflection could be seen in SAED, this reflection was not evident in the WAXS patterns.

The intense (302) reflections indicate that neighboring PBZO molecules in the a direction have a tendency to align with relative axial shifts of $^3/_4c$, the repeat distance along the chain axis (note that an axial translation of $+^3/_4c$ is equivalent to an axial translation of $-^1/_4c$).

With this assignment for the localized scattering intensity in mind, it is useful to reexamine the WAXS patterns in Figure 2. Notice that while the (302) reflection on the second layer line is strong, there is diffuse streaking on the first layer line. How could it be possible to have streaking on $l = 1$ if there are distinct reflections on $l = 2$?

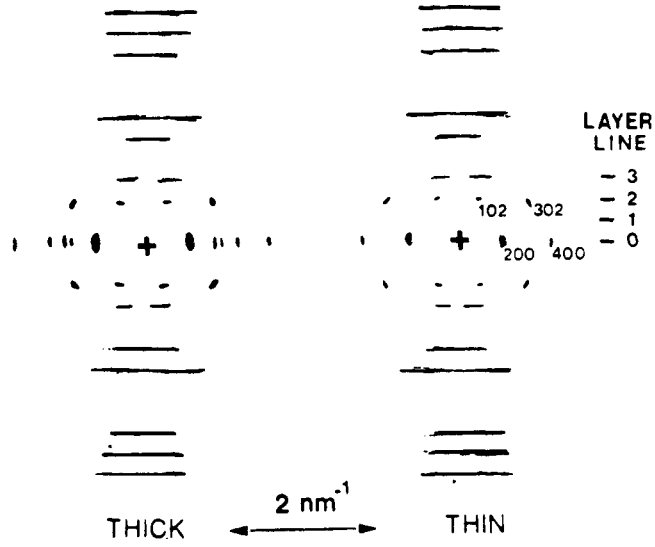

Figure 4. SAED patterns of PBZO from thick (a, left) and thin (b, right) fiber fragments. In some very thin sections it was possible to observe only the (200) and (400) equatorial reflections corresponding to single-crystal texturing about the [010] zone axis. It was observed that whenever (200) and (400) were visible, the localized reflections on the second layer line were also seen. This means it is possible to unambiguously index these reflections as (102) and (302), respectively. The (302) reflection corresponds to that seen in the WAXS patterns (Figure 2). Because of the predominance of inelastic scattering at low angles ($k < 0.8\ nm^{-1}$), analyzing the scattering behavior on the first layer line by SAED is problematic.

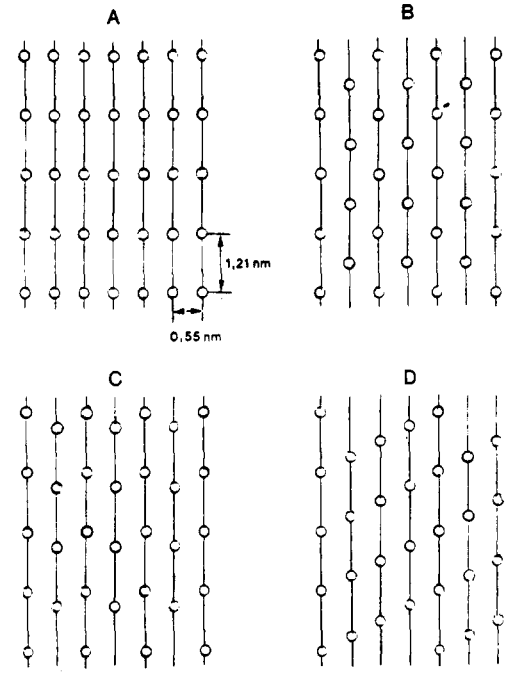

Figure 5. Models of different types of regular axial registry between PBZO molecules in the a–c plane. (A) Axial shift of 0c; (B) axial shift of $^1/_2c$; (C) axial shifts of $+^1/_4c$ and $-^1/_4c$; (D) axial shift of $+^1/_4c$.

Figure 5 shows several different models of axial registry between neighboring PBZO molecules in the a–c plane. Figure 5A shows a model with the neighboring chain at a shift of 0c. Figure 5B shows the neighboring chain at a shift of $^1/_2c$. Figure 5C shows a strictly alternating model with axial shifts of $+^1/_4c$ and $-^1/_4c$. Figure 5D shows a model with a regular placement of $+^1/_4c$.

Figure 6 shows the corresponding predictions of each of these models on the ($h0l$) scattering behavior of PBZO. Note that only models C and D, which have a regular

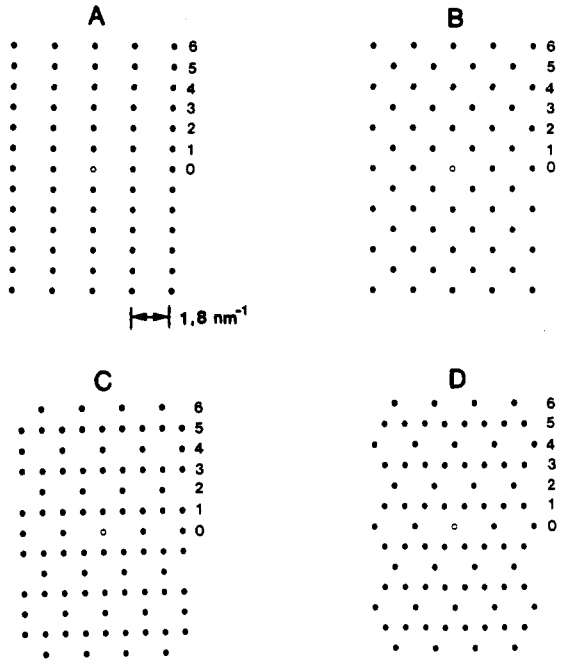

Figure 6. Reciprocal lattices corresponding to the axial shift models of Figure 5. (A) Axial shift of 0c; (B) axial shift of $^1/_2c$; (C) axial shifts of $+^1/_4c$ and $-^1/_4c$; (D) axial shift of $+^1/_4c$.

placement of $^1/_4c$ between neighboring PBZO molecules, correctly predict the experimentally observed scattering behavior on the second layer line with reflections at (102) and (302).

There are two plausible explanations for streaking on the first layer line, with localized reflections on the second layer line. First, it may be that there is a strong tendency for $^1/_4c$ registry to occur but that there is a high probability for this registry to be either $+^1/_4c$ or $-^1/_4c$. This means that the actual structure would be comprised of domains of variable width of type C and type D. Such a defect structure is reasonable because of the low energy of axial shift misregistry. A schematic comparing the expected diffraction pattern from this disorder model and that experimentally observed is shown in Figure 7.

Another possibility is that the streaking on the first layer line occurs because PBZO chains, which are well ordered axially in the a–c plane, are highly axially disordered in the b–c plane. It is possible to distinguish between this model and the combined $\pm^1/_4c$ shift model by examining the distribution of intensity on the first layer line in single-crystal textured samples. If streaking persists on $l = 1$ for single-crystal textured regions in the [010] zone, then this confirms the combined $\pm^1/_4c$ shift model. Unfortunately, the predominance of inelastic scattering makes analysis of the scattering at low scattering angles ($k = 0.8$ nm^{-1} for $l = 1$ at $R = 0$) difficult by conventional SAED. Future studies using energy-filtered SAED would be useful to resolve this question. WAXS requires the use of large samples, so it is not possible to distinguish between a and b axis disorder in a uniaxially symmetric fiber. WAXS would be useful if it were possible to induce single-crystal texturing in large fibers, perhaps by rolling deformation.

In summary, the crystal structure of PBZO consistent with our scattering data is one based on unit cells C and D with regular axial shifts of both $+^1/_4c$ and $-^1/_4c$ between neighboring PBZO molecules in the a direction. The projected electron potential of this unit cell in the [010] direction, showing the relative axial shifts of $+^1/_4c$ and $-^1/_4c$, is presented in Figure 8a. As is apparent from Figure

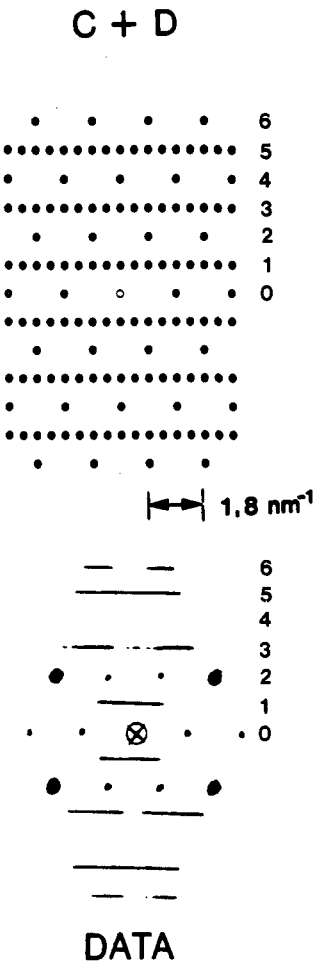

Figure 7. Combined pattern using models C and D. The reflections are coincident on even layer lines but interdigitated on odd layer lines. This suggests that a model having random $+^1/_4c$ and $-^1/_4c$ shifts between neighboring molecules would exhibit localized reflections on $l = 2$ but would show streaking on $l = 1$. A schematic of the experimental data (Figure 2) is also shown.

8a, the $^1/_4c$ placement allows the pendant hydrogens in the middle of the heterocyclic group to fit into gaps created by five-membered rings on the heterocyclic groups of neighboring PBZO molecules. Figure 8b also shows a theoretically predicted HREM image for a 10-nm thick section of PBZO with a similar orientation at Scherzer focus.[5] This image was calculated with the multislice technique,[17] assuming a microscope operating at 200 kV with a spherical aberration coefficient of the objective lens equal to 2.3 mm. Note that while the 0.55-nm planes can be easily seen, the details about the regular placement between molecules are difficult to distinguish.

Figure 8c shows the projected electron potential and Figure 8d a simulated HREM image of PBZO in the [001] direction, corresponding to a view down the chain axis. These figures illustrate the shape of the PBZO cross section and the nature of packing between chains. Experimentally, it has not yet been possible to obtain HREM images of PBZO down the chain axis.

Unit cell C corresponds to the monoclinic space group Pc (No. 7). It contains a symmetry element consisting of a glide plane oriented perpendicular to c with a glide vector of $a/2$. The unit cell parameters are $a = 1.120$ nm, $b = 0.354$ nm, $c = 1.205$ nm, and $\gamma = 101.3°$ with two repeat units per cell. The calculated density is 1.66 g/cm^3.

From this analysis we can state that a model involving regular axial shifts of $\pm^1/_4c$ between PBZO molecules close

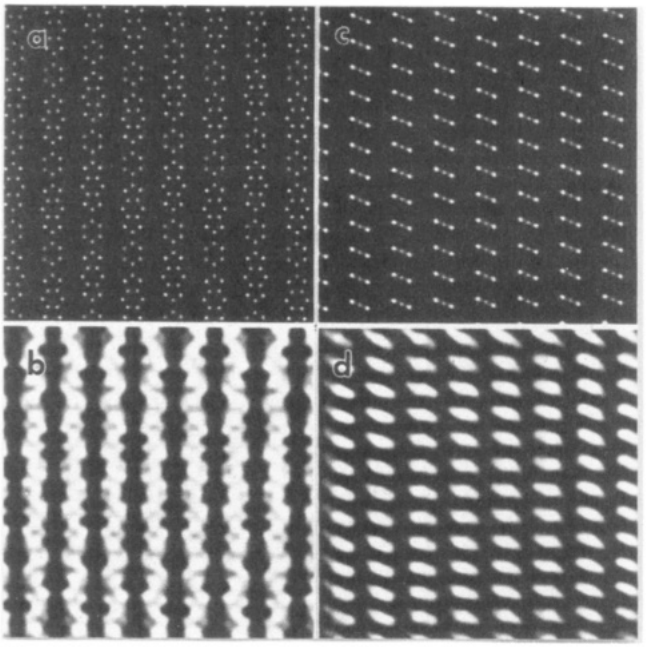

Figure 8. Projected electron potential and simulated images of PBZO for a JEOL 2000 FX at Scherzer focus and for 10-nm-thick samples. (a) Potential projected in the [010] direction for a model with regular placement of $+^1/_4c$ and $-^1/_4c$ between molecules in the a direction. (b) Simulated image in the [010] direction. (c) Projected potential in the [001] direction. (d) Simulated image in the [001] direction. The simulated images lack high-resolution detail but serve to unambiguously reveal the local orientation of the polymer chains. Near the Scherzer focus the contrast is reversed; areas of high projected potential (molecules) appear dark in the images.

packed edge to edge in the a direction is consistent with our WAXS and SAED data. The streaking that can be seen on certain layer lines is evidence that there is still a substantial amount of axial shift disorder in PBZO. However, the localized reflections on $l = 2$ indicate three-dimensionally ordered crystalline organization. One possibility presented here is that there is regular placement of neighboring PBZO molecules at $^1/_4c$ but there is disorder in terms of whether the placement will be at $+^1/_4c$ or at $-^1/_4c$. The precise characterization of this shift disorder will benefit from higher resolution HREM images than those obtained in this study (imaging the 0.32 nm (302) spacing would be most revealing), as well as a thorough comparison of more sophisticated models to better scattering data obtained by quantitative scans of PBZO layer lines with an X-Ray diffractometer.

2. HREM. The effect of electron beam irradiation on PBZO has been studied by Kumar and Adams.[18] During irradiation, the intensity and sharpness of the (001) meridional reflections persist even after the loss of sharp crystalline reflections on the equator, with the TEPD of the (003) reflection determined to be approximately 1.6 C/cm^2. This indicates that the damage mechanism involves the disruption of packing between molecules rather than the scission and reorientation of bonds along the fiber axis. This behavior is similar to that seen in PBZT and other oriented polymers and is consistent with the weak secondary forces between molecules and the strong covalent bonds along the polymer backbone.

It was possible to obtain HREM images of the 0.55-nm (200) and 0.35-nm (010) lattice spacings in fiber fragments of PBZO with various amounts of heat treatment.

Figure 9 is an HREM image of a detached fragment of a PBZO as-spun fiber. The crystallites are small but all are highly oriented with respect to one another. The

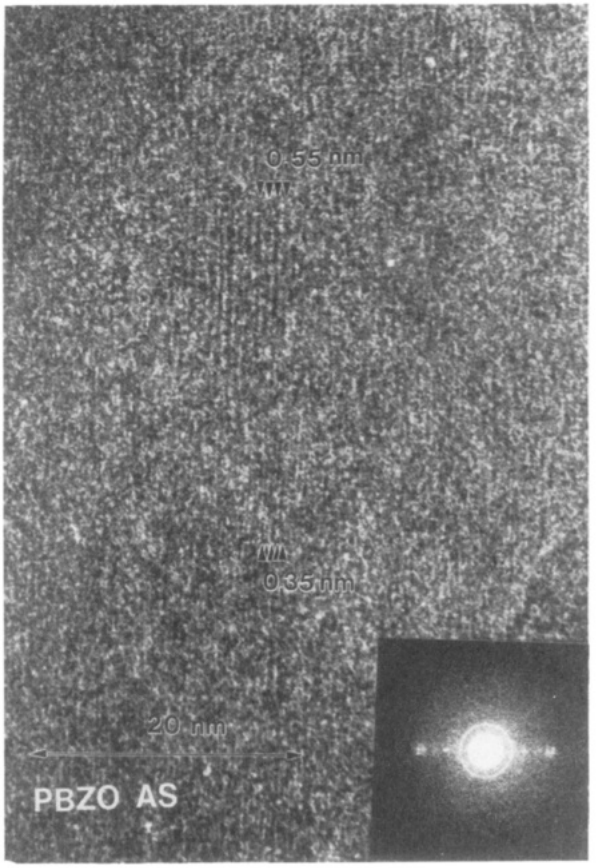

Figure 9. HREM image of as-spun PBZO. The crystallites are small and compact but are all highly oriented. The optical transform is inset showing both the 0.55-nm (200) and 0.35-nm (010) spacings. A slight indication for the 1.2-nm (001) layer line is also seen in the optical diffraction pattern.

optical transform of the image is inset. Careful inspection shows that there are fringe regions in the image that have low contrast and are axially oriented, corresponding to weak lateral ordering between PBZO molecules on a very local scale.

Figure 10 is an HREM image of a PBZO HT 600 fiber. Again, the crystallites are all highly oriented. However, in the heat-treated fiber the crystallites have a distinctly larger mean size. In some HREM images of heat-treated PBZO it was possible to find areas that were dominated by (200) fringes, with little or no evidence for (010) fringes. This suggests that these were regions exhibiting single-crystal orientation texturing like that seen in SAED. Figure 11 is an image of such a (200) fringe domain. This particular region is larger than the field of view of the enlargement (50 nm × 80 nm).

In PBZO HT 665, crystallites that were rather large in the lateral direction were sometimes seen. One such domain is shown in Figure 12. The crystallite in this image is approximately 40 nm in lateral extent. The streaking evident on the first layer line in the optical transform supports the random $\pm^1/_4c$ shift disorder model discussed earlier. Viewing this image at a glancing angle from below, it is possible to see that the left side of the crystallite is defective, with a local change in the orientation of the PBZO molecules of approximately 3–4° within 20 nm along the orientation direction. Laterally broad crystallites such as these support the DF studies of Adams et al.[7] and Krause et al.[8] which showed a tendency for PBZO crystals to grow more in the lateral than axial direction. However, it is not possible to determine the internal perfection of crystallites by DF.

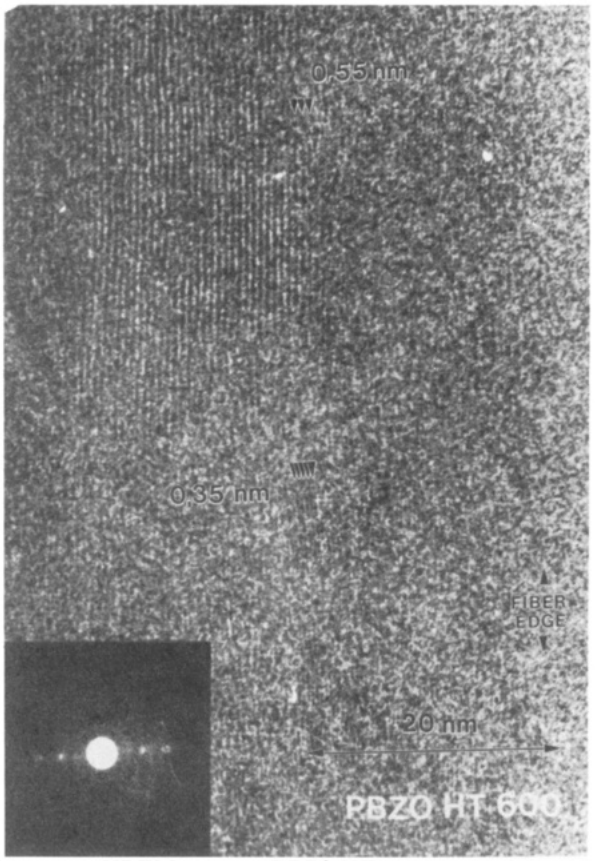

Figure 10. HREM image of PBZO HT 600. As for the as-spun fiber, the crystallites are all highly oriented. However, in this heat-treated sample the crystallites seem to be of a larger mean diameter. The optical diffraction pattern is inset.

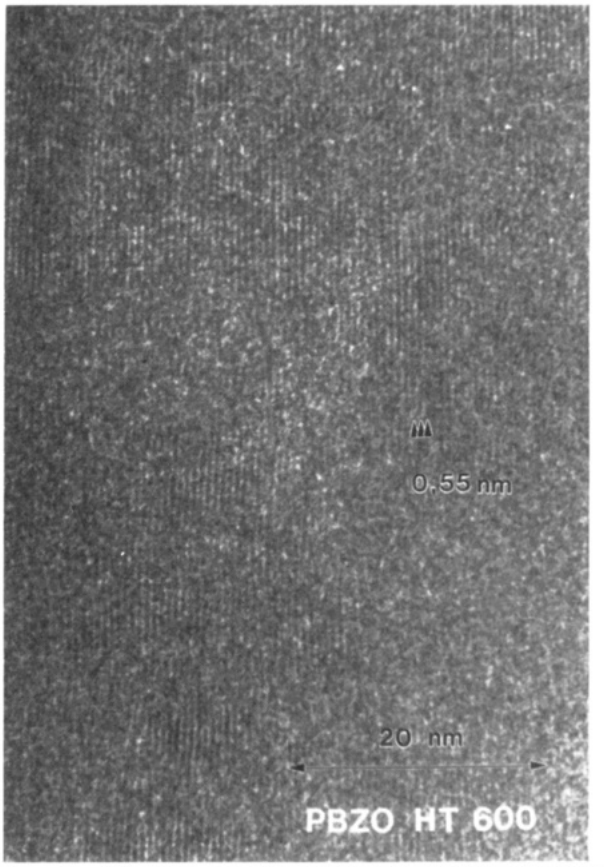

Figure 11. HREM image of a PBZO HT 600 fiber fragment showing a region with a high population of (200) fringes, supporting SAED data that showed single-crystal orientation texturing in thin sections. The optical diffraction pattern shows only the (200) reflections on the equator.

The characterization of orientation fluctuations is of considerable interest for understanding the properties of rigid-rod polymer fibers. For example, Argon has proposed a model for compressive strength of oriented composites in terms of a shear instability between locally misoriented units.[19] From our HREM images it was possible to characterize the complete, local orientation distribution of the PBZO molecular axis as a function of heat treatment. The results of such measurements are shown in Table II. It can be seen that like PBZT, PBZO is highly oriented on a local scale. However, as seen directly in images such as Figure 12, measurable deviations do exist; there is a standard deviation of about 1.3° of misorientation in all of the PBZO fibers studied. The amount of misorientation measured by HREM does not change significantly with heat treatment. The Hermanns-Stein orientation function is over 0.999 for all of the fiber samples. The orientation frequency distributions for the PBZO samples are presented and compared with those of PBZT in Figure 13. The orientation distributions are all indicative of uniform, uniaxial orientation.

In order to analyze the crystallite sizes, shapes, and orientations from these images, several enlargements were made of each sample and the boundaries of the fringe domains were determined by eye. The domains of fringes thus determined were relatively compact and limited in extent. No systematic "rhombohedral" or other unique shapes were seen. The maximum sizes of the domains determined in this way were measured in both the axial and lateral directions.

Figure 14 shows a plot of the crystal sizes in (a) as-spun PBZO fiber and (b) heat-treated PBZO fiber (HT 600 and HT 665) as determined by both HREM and DF. The DF data shown were collected both in this study and in the study by Adams et al.[7]

From these plots it is possible to measure the average lateral and axial crystallite size as a function of heat treatment. These results are shown in Table III. As suggested from Figure 14, the crystals grow in both the lateral and axial directions, although growth in the lateral direction is somewhat more extensive. The lateral crystallite size increases from an average of 7.8 nm for as-spun PBZO to 10.9 nm for HT 600 and 19.4 nm for HT 665. The average axial crystallite size increases from 10.2 for as-spun and HT 600 to 14.2 nm for HT 665. From these results we find that the average axial to lateral crystallite size ratio decreases systematically from 1.31 for as-spun to 0.93 for HT 600 and finally 0.73 for HT 665.

It is interesting to note that the average crystallite size determined for as-spun PBZO from HREM imaging (7.8–10.2 nm) is almost twice as large as that determined from DF images by Adams et al.[7] and Krause et al.[8] (5.2–5.4 nm). This discrepancy may reflect the fact that it is not possible to distinguish what are truly crystallites and what are statistical intensity fluctuations in DF imaging.[20] It might also indicate the fact that it is difficult to resolve small fringe patterns on low-dose HREM images.

It is also possible to measure an effective crystallize size from the broadening of spots in the optical transforms of the HREM images. As in a normal WAXS or SAED diffraction experiment, the average size of the crystallites is proportional to $D = 1/k_d$, where k_d is the full width at half-maximum of the diffracted intensity. The area on the micrograph selected with the laser beam for these measurements corresponded to a region of approximately

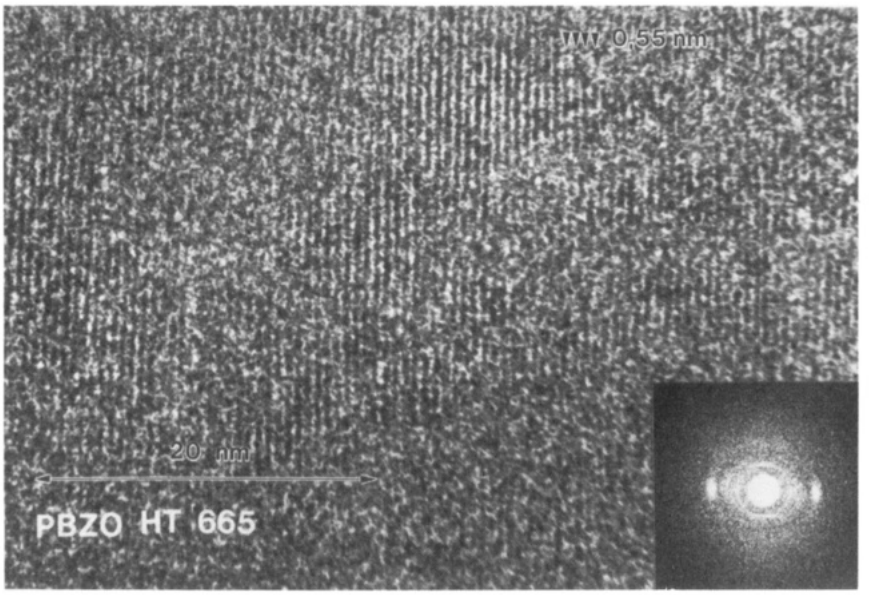

Figure 12. HREM image of PBZO HT 665 showing a domain that has grown quite large (~40 nm) in the lateral direction. The optical diffraction pattern is inset and shows a streaked reflection on the first layer line.

Table II
Orientation Measurements from HREM Images

fiber	standard dev, deg	no. of observations	Hermans-Stein orientation param
PBZT	1.26	85	0.999 27
PBZO AS	1.33	39	0.999 20
PBZO HT 600	1.43	65	0.999 30
PBZO HT 665	1.25	16	0.999 29

150 nm in diameter on the sample. It is possible to estimate both a lateral and axial size of the crystallites by measuring the reflections in directions perpendicular and parallel to the direction of molecular orientation, respectively. The results obtained are summarized in Table IV. The lateral size of the crystallites measured from broadening of the equatorial reflections in the optical diffraction patterns increases from 2.6 nm for the PBZO as-spun to 4.8 nm for PBZO HT 665. These sizes are only 24–33% of the size observed directly in the micrographs themselves. This indicates that the crystallites on the HREM negatives have internal disorder, which causes their optical diffraction spots to broaden.

Evident in some of the optical transforms of HREM images of PBZO was diffuse scattering on the 1.2-nm (001) first layer line. This confirms that, as in PBZT, there is a significant amount of axial disorder between neighboring molecules. The crystallite sizes measured from the layer lines in optical diffraction patterns (Table IV) indicate an extended axial size (13.7–19.6 nm) and a limited lateral size (0.8–0.9 nm). These results further support the assertion that when regular $\pm^1/_4c$ axial registry occurs between PBZO molecules, it does so in a random ± fashion. Unfortunately, it has not yet been possible to obtain high-quality images of the axial shift disorder in PBZO like those that have been obtained for PBZT.[5]

The true power of HREM imaging is in providing information about defect structures at a local level. In a particular HREM image of PBZO HT 600 there was a large crystallite that exhibited a (200) fringe that apparently terminated within the crystallite. This provides direct evidence for (but does not confirm) an edge dislocation with the Burgers vector perpendicular to the orientation axis. An enlarged view of this defective area is shown in Figure 15. Both the Burgers vector (0.55 nm in the [100] direction) and the direction of the dislocation

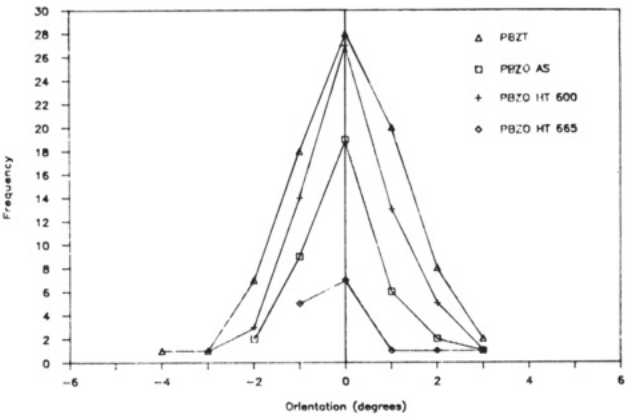

Figure 13. Plot of the crystallite orientation distribution of rigid-rod polymer fibers as determined directly by HREM. Although the fibers are all very highly and uniformly oriented, a certain measurable amount of misorientation does exist.

(approximately parallel to the [010] beam direction) are perpendicular to the fiber axis.

Figure 16 shows an arrangement of a layer of PBZO molecules that, if repeated on every layer within the thin section, would generate a dislocation with a precisely determined position of the core. Such a model does not seem physically reasonable, since it would require the cooperative segregation of a number of chain ends oriented in the same direction onto a single line. In fact, Figure 15 does not show a well-defined dislocation core region, suggesting that the direction of the dislocation is not strictly parallel to the electron beam. In the model, incorporating the dislocation into the crystallite requires an amount of tilt to be induced in one section of the crystal lattice. Close inspection of the HREM image, accomplished by viewing the micrograph at a glancing angle in the direction of the fringes, shows a similar tilting of the PBZO lattice near the actual defect.

Such an edge dislocation may serve as a nucleus for fracture or for the segregation of solvents and other impurities. Also, it may facilitate or frustrate certain slip systems of the PBZO crystallite during shear deformation. Since the Burgers vector and the dislocation orientation are both perpendicular to the chain axis, it is difficult to envision simple molecular mechanisms for the motion of

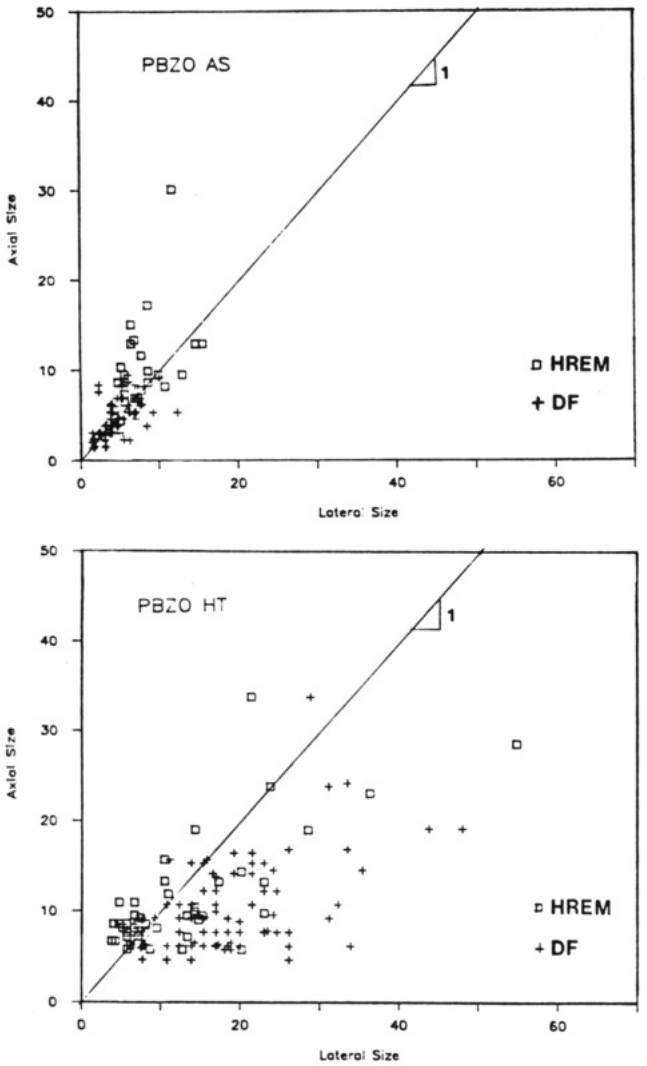

Figure 14. (a, Top) Crystallite size and shape distribution in as-spun PBZO as determined by HREM (nm). Results from DF measurements from this study and from the study of Adams et al.[7] are also shown. (b, Bottom) Crystallite size and shape distribution in heat-treated PBZO as determined by HREM (nm). Results from DF measurements from this study and from the study of Adams et al.[7] are also shown.

Table III
Crystallite Sizes (nm) As Determined from HREM Images

		lateral direction		axial direction	
fiber	N_{obs}	av	σ_d	av	σ_d
PBZT HT	46	10.4	4.0	17.2	8.0
PBZO AS	30	7.8	3.0	10.2	5.0
PBZO HT 600	35	10.9	7.2	10.2	5.4
PBZO HT 665	10	19.4	13.3	14.2	7.4

Table IV
Crystallite Sizes (nm) As Determined from Optical Diffraction Patterns

	equatorial		layer line	
fiber	lateral	axial	lateral	axial
PBZT	4.6	4.0	1.0	22.8
PBZO AS	2.6	3.0	0.9	13.7
PBZO HT 600	3.9	3.9		
PBZO HT 665	4.8	2.4	0.8	19.6

this dislocation without involving covalent bond bending or climb of an entire plane of molecules.

Images containing crystals with internal dislocation defects were uncommon. This is apparently because the average crystals are so small that most of the disorder is taken up in the grain boundary regions.

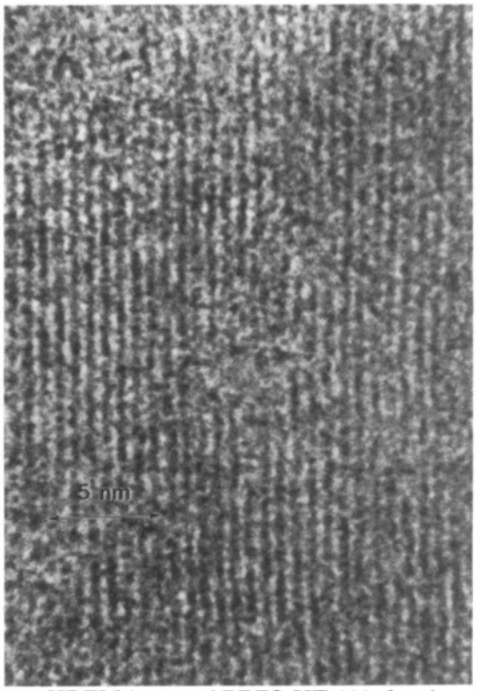

Figure 15. HREM image of PBZO HT 600 showing evidence for an edge dislocation. The direction of the dislocation is approximately parallel to the [010] viewing direction, and the Burger's vector is 0.55 nm in the [010] direction, corresponding to an extra (100) plane. The image is best viewed from a glancing angle along the direction of the fringes.

E. Discussion

It is of interest to compare the results about crystal size, size distributions, and shape for PBZT and PBZO with those for other materials. Theories and experimental data for normal grain growth in pure, single-phase systems have recently been reviewed by Atkinson.[21] Recent insight about the details of grain growth have been provided by 2-D Monte Carlo simulations,[22] which enable specific aspects about the grain size and shape distribution to be analyzed.[23]

The computer simulations show a frequency–grain size distribution that is peaked near the average grain size R_a.[23] The maximum grain size R_{max} is approximately $2.5R_a$, and the minimum size is about $0.1R_a$. Analysis of the growth rate of each grain as a function of size R/R_a shows that for grains larger than R_a the growth rate $d(R/R_a)/dt$ is randomly distributed about zero, whereas for small grains the rate becomes strongly negative. This indicates that small grains have a strong tendency to decrease in size, whereas large grains are both increasing and decreasing in size in a more or less random fashion.

The breadth of the crystal size distributions seen in HREM and DF for PBZT and PBZO are in general agreement with these results. However, the chain connectivity and extremely anisotropic nature of grain boundary energies suggest that the dynamics and energetics of grain boundaries in polymer solids will be significantly different than those of metals and oxides. In particular, the small crystallite size (~10 nm) means the defect density is high, so that the physical processes involved during heat treatment of PBZO fibers are more akin to recovery and recrystallization than normal grain growth.[24] Further investigations that provide more detailed information about structural evolution in ordered polymers will be important to elucidate the differences between metallic, ionic, and covalently bonded solids.

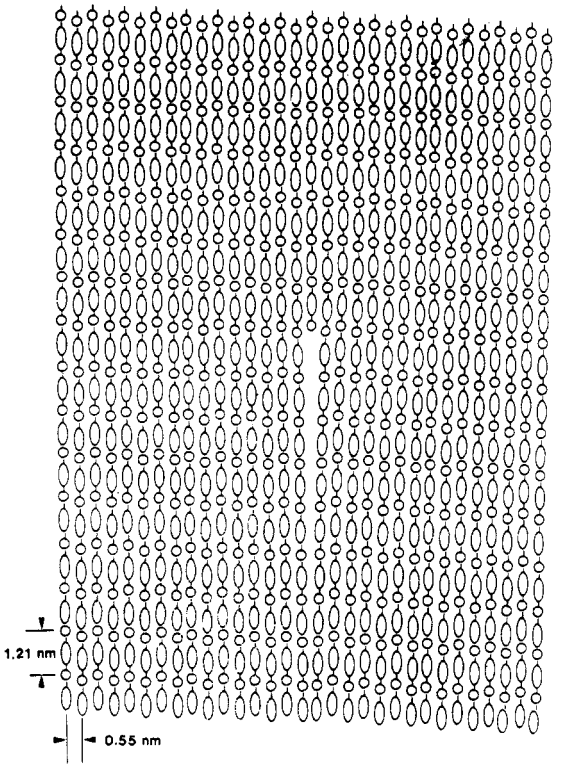

Figure 16. Schematic model of an edge dislocation involving an extra (100) plane, which might explain the HREM image in Figure 15. The circles represent the *p*-phenylene unit and the ellipses the heterocyclic benzobisoxazole group. The lack of a well-defined dislocation core in the image suggests the direction of the dislocation is not well-determined.

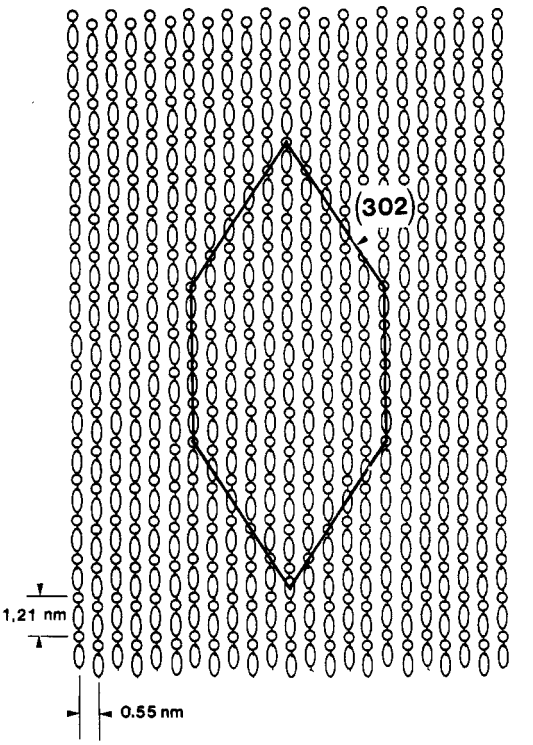

Figure 17. Schematic model to explain the origin of the four-point SAXS pattern of PBZO in terms of crystallites with regularly oriented axial chain invariant grain boundaries. As in Figure 16, the circles represent the *p*-phenylene unit and the ellipses the heterocyclic benzobisoxazole group. The preferred boundary planes are of the (302) type, whose WAXS reflections were seen to sharpen and increase in intensity after heat treatment (Figure 2).

Initial 2-D Monte Carlo simulations have shown that grain boundary energy anisotropy causes broadening of the crystal size distribution, giving rise to a microstructure with large grains and extended regions of small grains.[25] This anisotropy was also observed to decrease the grain growth kinetics and to give rise to grains with preferential shapes. Also, grain boundary anisotropy caused intergrain orientation correlations, but these correlations were limited to a few times R_a for the potentials used.[25]

It is appropriate to discuss here an observation that was NOT made in this study that might have been expected. The SAXS patterns by Adams and Grubb[9] indicate that PBZO fiber has a tendency to develop periodic fluctuations in electron density at specific angles to the fiber axis. The characteristic dimension of the four-point patterns is on the order of 8 nm, and the diffuse regions of diffracted SAXS intensity make an angle of approximately 57° with the fiber axis.[7,9]

This characteristic dimension of the SAXS scattering (8 nm) corresponds approximately with the average size of a PBZO crystallite (10 nm). Therefore, it seems reasonable that the four-point SAXS patterns arise from arrangements of crystallites that have a preferential shape. In particular, it seems reasonable that axial grain boundaries of PBZO crystallites could have a propensity to be oriented at specific angles to the fiber axis. From WAXS, we found that there were sharp reflections due to good packing in (302) planes. Notably, these strong (302) reflections make an angle of 57° with the fiber axis. This suggests that the (302) planes may have a dominant role in the origin of the four-point pattern. A specific model is that the (302) planes often serve as axial grain boundaries for PBZO crystallites. A schematic of such a PBZO crystallite with (302) faces is shown in Figure 17. Calculations of the shape transform of such a crystallite show a four-point pattern that is similar to that of the PBZO SAXS data. A theoretical analysis of the SAXS scattering of polymer crystallites with different characteristic shapes has been presented by Asherov and Ginzburg.[26] The question is, if this model is correct, why are such regular grain boundary shapes not visible in HREM and DF studies?

One explanation for the lack of observation of crystallites with a unique shape by HREM is that the axial grain boundaries are simply not localized and flat enough to give interpretable projections. Another is that the crystallite boundaries may not be oriented in a useful projection direction when (200) or (010) fringes can be seen. Finally, it might be that we simply have not yet obtained enough images to find a region of the sample in which the supposed characteristic shape of the PBZO crystallites can be clearly seen.

It should be noted that it IS possible to find rhombohedral-shaped crystallites in poly(*p*-phenyleneterephthalamide) (PPTA) thin films. A recent study showed rhombohedral crystals for PPTA/sulfuric acid solutions that were sheared and then slowly coagulated by exposure to atmospheric moisture.[27] The axial boundaries of the crystallites observed by optical microscopy (OM) and TEM were inclined at a significant angle (approximately 55°) to the axis of orientation of the PPTA molecules. It was thought that these structures were representative of a crystal solvate phase that formed during slow coagulation. Although a physical explanation for the rhombohedral shapes was not discussed, they apparently arise because of low-energy axial grain boundaries which prefer to form at specific orientations with the molecular axis.

In summary, we have found that the ultrastructure of PBZO fibers consists of discrete, uniaxially oriented crys-

tallites. The small size of these crystallites (7–20 nm) means structural defects such as grain boundaries between and dislocations within crystallites may play an important or even dominant role in determining the unique properties of these materials. On the basis of these observations, future studies of the structure, energetics, and influence on properties of particular boundary defects should facilitate a more detailed understanding of the properties of extended-chain polymer fibers.[28]

F. Conclusions

WAXS and SAED patterns of PBZO show an increase in three-dimensional crystallinity as a function of heat treatment. There is a strong off-axis reflection on the second-order layer line, which increases in intensity and becomes more localized as the fibers are heat-treated.

Thin sections of PBZO exhibit single-crystal texturing with the [010] direction parallel to the electron beam, indicating a tendency for the PBZO molecules to lie "flat" in the plane of the detached film. This phenomena enables the strong off-axis reflections to be indexed as (302), corresponding to regular axial registry of $\pm^1/_4c$ between molecules in the a direction.

The new unit cell proposed for PBZO is based on the monoclinic space group Pc (No. 7). The unit cell parameters are a = 1.120 nm, b = 0.354 nm, c = 1.205 nm, and γ = 101.3° with two repeat units per cell. The calculated density is 1.66 g/cm^3.

HREM images of PBZO show 0.55-nm (200) and 0.35-nm (010) fringes corresponding to the closest lateral packings between molecules. This size, shape, and relative orientation of PBZO crystallites can be directly determined from these images.

The average lateral crystallize size increases from 7.8 nm for as-spun PBZO to 10.9 nm for HT 600 and 19.4 nm for HT 665. The ratio of the average axial size to average lateral size decreases from 1.31 for as-spun to 0.93 for HT 600 to 0.73 for HT 665.

The orientation distributions indicate high, uniform orientation of the PBZO molecules parallel to the fiber axis, with a standard deviation of approximately 1.3°. Certain instances of significant local misorientation (3–4° within 20 nm in Figure 12) are observed. The local degree of orientation determined by HREM does not vary significantly as a function of heat treatment.

Crystallite sizes determined by the breadth of spots in the optical transform (2.6–4.8 nm) are three to four times smaller than those determined directly from HREM images (7–20 nm). This suggests that the PBZO crystallites have disorder within them that causes the optical diffraction spots to smear more than can be attributed solely to crystallite size.

Evidence for an edge dislocation defect oriented in the [010] direction with a Burgers vector of [100] was observed within a PBZO crystallite. In this type of edge dislocation both the dislocation direction and Burgers vector are perpendicular to the primary axis of orientation. Such a defect could be formed by the mutual segregation of a number of similarly oriented chain ends along the dislocation line.

Acknowledgment. D.C.M. thanks the Shell Co. for a Doctoral Research Fellowship. Helpful comments and samples were provided by W. Wade Adams of WPAFB. E.L.T. thanks the AFOSR for financial support through Grants 85-0275 and F49620-89-C-0073. This paper is dedicated to the memory of Dr. D. R. Ulrich, AFOSR.

References and Notes

(1) Wolfe, J. F.; Sybert, P. D.; Sybert, J. R. U.S. Patent 4 553 693, 1985.
(2) Weirshke, S. G. In *The Materials Science and Engineering of Rigid-Rod Polymers*; Adams, W. W., Eby, R. K., McLemore, D. E., Eds.; Materials Research Society Symposia Proceedings, 134, 1989; pp 313–327.
(3) Won Choe, E.; Kim, S. N. *Macromolecules* **1981**, *14*, 920–924.
(4) Bhaumik, D.; Welsh, W. J.; Jaffe, H. H.; Mark, J. E. *Macromolecules* **1981**, *14*, 951–953.
(5) Roche, E. J.; Takahashi, T.; Thomas, E. L. In *Fiber Diffraction Methods*; French, A. D., Gardner, K. G., Eds.; ACS Symposium Series 141; American Chemical Society: Washington, DC, 1980; pp 303–313.
(6) Fratini, A. V.; Adams, W. W. *Am. Cryst. Assoc. Abs.* **1985**, *13*, 72.
(7) Adams, W. W.; Grieshop, T.; Helminak, T.; Hunsaker, M.; O'Brien, J. F.; Altieri, M.; Bai, S. J.; Brandt, M.; Fratini, A. V.; Hwang, W.-F.; Price, G. E.; Soloski, E.; Haddock, T.; Krause, S. J.; Lenhert, P. G. AFWAL-TR-86-4011, 1986.
(8) Krause, S. J.; Haddock, T. B.; Vezie, D. L.; Lehnert, P. G.; Hwang, W.-F.; Price, G. E.; Helminiak, T. E.; O'Brien, J. F.; Adams, W. W. *Polymer* **1988**, *29*, 1354.
(9) Adams, W. W.; Grubb, D. T., unpublished results.
(10) Minter, J. R. Structural Investigations of Fibers and Films of Poly(*p*-phenylene benzobisthiazole). Ph.D. Dissertation, University of Massachusetts at Amherst, Amherst, MA, 1982.
(11) Adams, W. W.; Kumar, S.; Martin, D. C.; Shimamura, K. *Polym. Commun.* **1989**, *30*, 285–287.
(12) Young, R. J.; Day, R. J.; Zakikhani, M. *J. Mater. Sci.* **1990**, *25*, 127–136.
(13) Fratini, A. V.; Lenhert, P. G.; Resch, T. J.; Adams, W. W. In *The Materials Science and Engineering of Rigid-Rod Polymers*; Adams, W. W., Eby, R., McLemore, D., Eds.; Materials Research Society Symposia Proceedings 134, 1989; pp 465–474.
(14) As reported to W. Wade Adams of WPAFB by H. Ledbetter, Dow Chemical U.S.A., 1987.
(15) Martin, D. C. Direct Imaging of Deformation and Disorder in Extended-Chain Polymers. Ph.D. Dissertation, The University of Massachusetts at Amherst, Amherst, MA, 1990.
(16) Martin, D. C.; Thomas, E. L. *Mater. Res. Soc. Bull.* **1987**, *XII* (8), 27–37.
(17) Cowley, J. M.; Moodie, A. F. *Acta Crystallogr.* **1957**, *10*, 609–619.
(18) Kumar, S.; Adams, W. W. *Polymer* **1990**, *31*, 15–19.
(19) Argon, A. S. Fracture of Composites. In *Treatise on Materials Science and Technology*; Academic Press: New York, 1972; Vol. 1.
(20) Thomas, E. L.; Roche, E. J. *Polymer* **1979**, *20*, 1413–1422.
(21) Atkinson, H. V. *Acta Metall.* **1988**, *36* (3), 469–491.
(22) Anderson, M. P.; Srolovitz, D. J.; Grest, G. S.; Sahni, P. S. *Acta Metall.* **1984**, *32* (5), 783–791.
(23) Srolovitz, D. J.; Anderson, M. P.; Sanhi, P. S.; Grest, G. S. *Acta Metall.* **1984**, *32* (5), 793–802.
(24) Reed-Hill, R. E. *Physical Metallurgy Principles*, 2nd ed.; Brooks/Cole Engineering Division, 1973.
(25) Grest, G. S.; Srolovitz, D. J.; Anderson, M. P. *Acta Metall.* **1985**, *33* (3), 509–520.
(26) Asherov, B. A.; Ginzburg, B. M. *Polym. Sci. U.S.S.R.* **1978**, *20*, 1719–1728.
(27) Roche, E. J.; Allen, S. R.; Gabara, V.; Cox, B. *Polymer* **1989**, *30*, 1776–1784.
(28) Martin, D. C.; Thomas, E. L.; *Philos. Mag.*, to appear.

Registry No. PBZO (SRU), 60871-72-9.